

Diffusion of iron in aluminum studied by Mössbauer spectroscopy

S. Mantl

*Institut für Festkörperforschung, Kernforschungsanlage Jülich GmbH,
Postfach 1913, D-5170 Jülich, Germany*

W. Petry

*Hahn-Meitner-Institut für Kernforschung Berlin GmbH und Freie Universität Berlin,
Glienickestrasse 100, D-1000 Berlin 39, Germany*

K. Schroeder

*Institut für Festkörperforschung, Kernforschungsanlage Jülich GmbH,
Postfach 1913, D-5170 Jülich, Germany*

G. Vogl

*Hahn-Meitner-Institut für Kernforschung Berlin GmbH und Freie Universität Berlin,
Glienickestrasse 100, D-1000 Berlin 39, Germany*

(Received 19 November 1982)

The broadening of the ^{57}Fe Mössbauer line due to diffusion jumps of the Fe atoms in an Al single crystal has been measured as a function of crystal orientation. The broadening is strongly anisotropic. Theoretical calculations for the broadening using the five-frequency model for the motion of an Fe atom via vacancies show that the following information about the geometry and perturbed jump frequencies of the Fe-vacancy complex can be obtained: (i) The anisotropy of the broadening yields information about the jump geometry and jump-frequency ratios, (ii) the absolute value and the temperature dependence of the broadening yield the diffusion coefficient and the activation energy for Fe diffusion, and (iii) the anomalous decrease of the Mössbauer intensity in the vicinity of the melting point yields information about the binding energy of the Fe-vacancy complex. Our results are consistent with the following interpretation: Fe in Al moves by exchanging sites with nearest-neighbor vacancies. The binding energy of an Fe-vacancy complex is $E_b \leq 0.29$ eV. The diffusion coefficient of Fe in Al is $D_{\text{Fe}} = 1.1 \times 10^{4 \pm 1} \exp[-(2.3 \pm 0.2 \text{ eV})/k_B T] \text{ cm}^2 \text{ s}^{-1}$ in reasonable agreement with results from tracer experiments. Values are obtained for different jump frequencies of a vacancy in the vicinity of an Fe atom.

I. INTRODUCTION

There is general agreement that vacancies are responsible for self-diffusion and impurity diffusion in most cubic metals.¹ Diffusion coefficients are usually measured by the tracer-diffusion technique. When suitable isotopes are available from studies of the isotope effect² the correlation factor can be deduced. This yields information on the atomistic mechanism for self-diffusion. Impurity diffusion is more complicated, since the jump frequencies of the defect may be changed in the neighborhood of the

impurity. From tracer-diffusion studies jump-frequency ratios can be determined.^{3,4} It is, however, not possible to measure the jump frequencies and to determine the elementary diffusion jump in a direct way.

Additional information can be obtained with methods which study defects and diffusion on an atomistic scale. We report here on an investigation of diffusion by Mössbauer spectroscopy. The influence of diffusion on the Mössbauer effect was described by Singwi and Sjölander⁵ and Krivoglaz.⁶ The physical picture used to describe classical dif-

fusion in a lattice is as follows: Most of the time an atom sits in an equilibrium position. By thermal fluctuations it gains so much energy that it is able to overcome the barrier for a jump into a neighboring empty lattice site. The duration of the jump is determined by the duration of a lattice vibration whereas the average time between two jumps (residence time) is much larger. If a Mössbauer atom (MA) performs one or more diffusion jumps during the lifetime of its excited nuclear state, the emitted γ ray is cut into pieces which are emitted from different sites. The absorbing nucleus records the phase shifts between the different parts of the γ ray. The distribution of residence times leads to an energy broadening of the nuclear resonance inversely proportional to the mean residence time τ . Since the jumps are thermally activated the mean residence time τ decreases with increasing temperature and thus the broadening increases. If the MA performs jumps on a discrete lattice the phase shifts of the emitted γ ray depend on the angle between the direction of emission (\vec{k} vector) and the lattice directions. Thus, the anisotropy of the line broadening which can be measured in a single crystal is characteristic of the geometry of the diffusion lattice.

Chudley and Elliot⁷ were the first to calculate the anisotropy of the line broadening due to discrete jumps in space for the case of ideal interstitial diffusion (uncorrelated jumps in an empty lattice). Later Krivoglaz and Repetskiy⁸ calculated the anisotropy of the line broadening due to diffusion via nearest-neighbor (NN) vacancies but they also neglected correlation effects. More recently, self-diffusion of the MA via NN vacancies including the effects of geometrical correlation between the jumps of a vacancy and the MA have been considered by Dibar-Ure and Flinn⁹ and Wolf¹⁰ in computer simulations and by Bender and Schroeder¹¹ in analytical calculations.

Besides this broadening, the diffusion of a MA causes relaxations of the hyperfine interactions due to changes in the hyperfine parameters. Such changes could be caused, e.g., by an approaching vacancy, since a vacancy in the immediate vicinity of the MA could change the electron density at the Mössbauer nucleus (measured by the isomer shift)

and cause an electrical field gradient (measured by a quadrupole splitting of the resonance).

The first Mössbauer *experiments* on diffusion were performed by Knauer and Mullen, who studied the diffusion of Fe impurities in polycrystalline Cu and Au.¹² Other authors studied the diffusion of Fe in various fcc and bcc hosts.¹³⁻¹⁷ All experiments yielded diffusional broadening of the Mössbauer resonance of the order of magnitude as expected from tracer diffusion. All were performed on polycrystalline specimens, therefore no information about the geometry of the diffusion lattice was obtained.

Just recently, two groups have performed *single-crystal* measurements of the anisotropic resonance broadening. Asenov *et al.*¹⁸ have studied the diffusion of ⁵⁷Fe in a Cu single crystal and Mantl *et al.*¹⁹ have reported on ⁵⁷Fe diffusion measurements in an Al single crystal. First evaluations of the measured anisotropy confirmed that in these systems diffusion takes place via NN vacancies. Considerable deviations were found, however, from theoretical calculations for self-diffusion as, for instance, performed by Bender and Schroeder.¹¹

In order to contribute to the atomistic understanding of impurity diffusion we reconsider in Sec. II the diffusion of a MA in an fcc host lattice in terms of the five-frequency model.³ In particular we consider the influence of binding between a vacancy and the MA on the diffusional broadening and on the relaxation of the isomer shift. Section III deals with the experimental procedure. Section IV presents more experimental data on ⁵⁷Fe diffusion in Al single crystals which are discussed in the light of the theory. We determine the elementary jump vector for diffusion and obtain microscopic information about the perturbed jump frequencies of a vacancy in the neighborhood of an Fe atom.

II. THEORY

Singwi and Sjølander⁵ have shown that the emission probability of γ rays from a diffusing Mössbauer atom (MA) can be expressed in terms of the diffusional part of the self-correlation function for the MA, $G_D(\vec{R}^{\vec{n}}, t)$:

$$\sigma_e(\vec{k}, \omega) = f_v \text{Re} \frac{1}{\pi \hbar} \int_0^\infty dt e^{-i\omega t - \Gamma_0 |t|/2\hbar} \sum_{\vec{n}} e^{i\vec{k} \cdot \vec{R}^{\vec{n}}} e^{i\omega_0 t} G_D(\vec{R}^{\vec{n}}, t). \quad (1)$$

Here \vec{k} is the wave vector and $\hbar\omega$ the energy of the emitted γ rays, $\hbar\omega_0 = E_e - E_g$ the energy of the nuclear transition, and Γ_0 is the natural linewidth of the excited state of the Mössbauer nucleus. The sum is over all equilibrium sites $\vec{R}^{\vec{n}}$ of the MA on a

discrete lattice. The Debye-Waller factor f_v describes the reduction of the intensity due to vibrations of the MA on one lattice site.

Expression (1) is correct if the jump rate of the diffusing MA is small compared to the frequencies

of vibration, and if any influence of the fluctuating environment on the nuclear-transition-like changes of isomer shift or quadrupole splitting can be neglected.

If one has to take into account influences of a fluctuating environment a much more complicated theory along the lines of Blume and Tjon²⁰ and Datagupta²¹ has to be employed. We shall present the

$$\sigma_e(\vec{k}, \omega) = f_v \text{Re} \frac{1}{\pi \hbar} \int_0^{+\infty} dt e^{-i\omega t - \Gamma_0 |t|/2\hbar} \sum_{\vec{n}} e^{i\vec{k} \cdot \vec{R}^{\vec{n}}} \langle e^{-i\epsilon_\alpha t/\hbar} G_D^\alpha(\vec{R}^{\vec{n}}, t) \rangle. \quad (2)$$

Here the index $\alpha=0,1,\dots$ specifies the possible isomer states of the Mössbauer nucleus with transition energies $\epsilon_\alpha = \hbar\omega_\alpha$ and enclosure by the angular brackets means taking the thermal average over these states. Explicitly the average reads

$$\langle e^{i\epsilon_\alpha t/\hbar} G_D^\alpha(\vec{R}^{\vec{n}}, t) \rangle = \sum_{\alpha, \beta} e^{-i\epsilon_\alpha t/\hbar} G_D^{\alpha\beta}(\vec{R}^{\vec{n}}, t | \vec{R}^{\vec{n}'}, 0) p_\beta, \quad (3)$$

where

$$G_D^{\alpha\beta}(\vec{R}^{\vec{n}}, t | \vec{R}^{\vec{n}'}, 0) = G_D^{\alpha\beta}(\vec{R}^{\vec{n}} - \vec{R}^{\vec{n}'}; t)$$

is the joint probability that during the time interval t the MA has migrated from site $\vec{R}^{\vec{n}'}$ to site $\vec{R}^{\vec{n}}$ and that the isomer state has changed from β to α . p_β is the *a priori* probability to find the MA in the isomer state β . To calculate $G_D^{\alpha\beta}(\vec{R}^{\vec{n}}, t)$ one has to describe the dynamics of the MA and of the surrounding vacancies separately for the various isomer states and the transitions between them. In the simplest model we assume an isomer shift only if a vacancy is in the NN shell of a MA (associated pairs) and no isomer shift for all vacancies which are further apart (nonassociated pairs). We can neglect configurations with more than one vacancy in the NN shell since in metals the vacancy concentration is always small ($< 10^{-3}$), even at the melting temperature. Then we have the following schematic picture for the dynamics of the Mössbauer nucleus (see Fig. 1): At $t=0$, a MA sits on site, say n' , and the vacancies are distributed according to thermal equilibrium. Even if due to interaction between vacancies and MA the vacancy distribution is inhomogeneous, for small binding energies (compared to the formation energy of a vacancy) most MA are in the nonassociated state (a). At elevated temperature the vacancies start to migrate and can jump to the NN shell of a MA thus changing the isomer state to the associated state (b). In this state the vacancy can induce a finite number of jumps of the MA during a short-time interval (c);

result of such a calculation for the case of diffusion of a substitutional MA via vacancies, e.g., Fe in Al, where the approaching vacancies can cause an isomer shift of the transition energy.²² Details of this calculation will be published separately.²⁴ The formula for the emission probability has to be modified to the form

the larger the binding energy the more jumps. Eventually the vacancy leaves the MA (d) and the isomer state changes to the nonassociated state.

There are essentially two models worked out in detail to describe the dynamics of a MA due to diffusion via vacancies. Both use different approximations. The first one, the so-called "encounter model," was originated by Eisenstadt and Redfield²⁵ and has been generalized by Wolf²⁶ and recently by Bender and Schroeder.¹¹ In its most sophisticated version it is capable of describing the dynamics of a MA-vacancy pair in detail, including the correlation effects due to geometry and binding.²⁷ However, this model has been explicitly applied only in a static approximation assuming instantaneous atom transfer due to all jumps induced by one vacancy (the "encounter") and neglecting the temporal development of these jumps. In this approximation²⁸ the model cannot describe the influence of isomer shift due to associated NN vacancies. In particular it *only describes one line* which carries all the intensity. It is, however, suited well to describe spatial correlations and thus the anisotropy of the

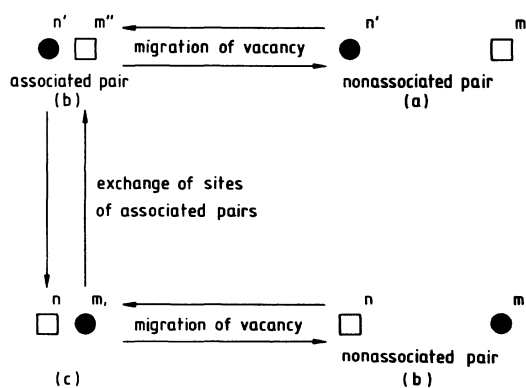


FIG. 1. Schematic picture of the possible transitions of the Mössbauer atom (●) via jumps of a single vacancy (□).

linewidth of the Mössbauer line for the nonassociated state, which we call the no-vacancy line.

The second model by Krivoglaz and Repetskiy⁸ explicitly describes the transition of vacancies between NN and other shells but *neglects the correlation due to repeated visits* of the NN shell. It can be easily adapted to include the isomer shift of the Mössbauer line for the associated state, which we call the vacancy line. Thus it can be used to describe the intensity of the two lines as a function of vacancy concentration and binding energy. However, due to the neglect of correlation effects the description of the anisotropy of the no-vacancy line is less accurate and general.

In the following we shall first discuss the results of the Krivoglaz model adapted to include isomer shift for the intensity and linewidth of the two-line spectrum, and then turn to the more complete description of the linewidth of the no-vacancy line in the encounter model.

A. The Krivoglaz-Repetskiy model including isomer shift

Krivoglaz and Repetskiy⁸ have discussed the dynamics of MA-vacancy pairs in fcc crystals. Owing to interaction effects the equilibrium concentration of vacancies in the nearest-neighbor shell and the vacancy jump frequencies are perturbed in the neighborhood of the MA as indicated in Fig. 2 using the nomenclature of Le Claire³ for the so-called five-frequency model. To simplify the analysis it is assumed that the rotation of vacancies in the NN shell of the MA is the fastest process, i.e., $w_1 \gg w_2, w_3$. Then any vacancy arriving at a NN site is quickly distributed over all sites of the NN shell, and after an exchange of sites between a vacancy and a MA (with frequency w_2) the vacancy is instantaneously distributed over the NN shell of the new MA position. In addition, it is assumed that a vacancy which has left the NN shell (with frequency w_3) loses its memory and is treated as one of the randomly distributed nonassociated vacancies. With these assumptions any correlation between the jumps of the MA and a vacancy is lost and only two configurations of a MA-vacancy pair can be distinguished: the associated state with a vacancy in the NN shell and the nonassociated state with no vacancy in the NN shell. For small vacancy concentrations we can neglect configurations with two or more vacancies in the NN shell. For more general jump-frequency ratios (small w_1) a distinction of the 12 possible orientations of the associated pairs is necessary and correlation effects can be described.

The equations governing the probabilities $G_D^{\alpha\beta}(\vec{R}^{\vec{n}}, t)$ read in the Krivoglaz model

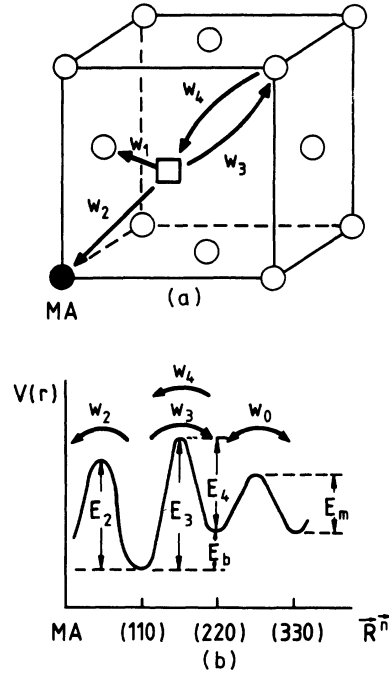


FIG. 2. (a) Five-frequency model for impurity diffusion in an fcc crystal. The vacancy jump frequencies are as follows: w_0 , vacancy jump in the pure host lattice; w_1 , vacancy jumps in the NN shell of the impurity atom; w_2 , exchange jump of vacancy with impurity atom; w_3 , dissociation jump out of the NN shell; w_4 , association jump into the NN shell. (b) Possible energy barriers for vacancy jumps in radial direction. The five frequencies can be parametrized by the corresponding five activation energies to overcome the potential barrier (E_1 not shown). $E_b = E_3 - E_4 =$ impurity-vacancy binding energy, $E_0 = E_m =$ migration energy.

$$\frac{\partial}{\partial t} G_D^{\alpha\beta}(\vec{R}^{\vec{n}}, t) + \sum_{\vec{m}, \alpha'} W_{\vec{n}\vec{m}}^{\alpha\alpha'} G_D^{\alpha'\beta}(\vec{R}^{\vec{m}}, t) = \delta(t) \delta_{\vec{n}, \vec{0}} \delta_{\alpha\beta}. \quad (4)$$

The transition matrix $W_{\vec{n}\vec{m}}^{\alpha\alpha'}$ describes the rates of transition from one configuration to another. It consists of two parts:

$$W_{\vec{n}\vec{m}}^{\alpha\alpha'} = W_0^{\alpha\alpha'} \delta_{\vec{n}\vec{m}} + \delta_{\alpha 1} \delta_{\alpha' 1} \frac{w_2}{Z} (Z \delta_{\vec{n}\vec{m}} - s_{\vec{n}\vec{m}}). \quad (5)$$

The first part

$$W_0 = \begin{pmatrix} 12c_v 7w_4 & -7w_3 \\ -12c_v 7w_4 & 7w_3 \end{pmatrix} \quad (6)$$

describes the change of the isomer state of a MA fixed on site $\vec{R}^{\vec{n}}$ due to association and dissociation

of vacancies to and out of the NN shell. (Here and in the following we have indicated the 2×2 matrices by a single underline.) The association can take place to any of the 12 NN sites with jump frequency w_4 from 7 different non-NN sites which are assumed to be occupied by vacancies with the vacancy concentration c_v as in the ideal crystal. The dissociation can take place from any site of the NN shell to seven different non-NN sites with jump frequency w_3 . The association and dissociation jump frequencies are related via the binding energy which also relates the NN-vacancy concentration c_{NN} to the non-NN-vacancy concentration:

$$\frac{w_3}{w_4} = \frac{c_v}{c_{NN}} = e^{-E_b/k_B T}. \quad (7)$$

Here E_b is the binding energy²⁹ of the MA-vacancy pair. The second term in Eq. (5) describes the motion of the MA due to exchange of sites with an associated vacancy. Z is the coordination number and

$$s_{\vec{n}\vec{m}} = \begin{cases} 1 & \text{if } \vec{R}^{\vec{n}} \text{ and } \vec{R}^{\vec{m}} \text{ are nearest neighbors} \\ 0, & \text{otherwise.} \end{cases}$$

The solution of Eq. (4) can be found by Fourier transformation $t \rightarrow \omega$, $\vec{R}^{\vec{n}} \rightarrow \vec{k}$ yielding a 2×2 matrix equation

$$-i\omega \underline{\tilde{G}}_D(\vec{k}, \omega) + \underline{\tilde{W}}_{\vec{k}} \underline{\tilde{G}}_D(\vec{k}, \omega) = \underline{\mathbb{1}} \quad (8)$$

with the formal solution

$$\underline{\tilde{G}}(\vec{k}, \omega) = (-i\omega \underline{\mathbb{1}} + \underline{\tilde{W}}_{\vec{k}})^{-1}. \quad (9)$$

$$\sigma_e(\vec{k}, \omega) = f_v \frac{1}{2\pi\hbar} \text{Re} \sum_{\alpha, \beta} \left\{ \left[\left[-i\omega + \frac{\Gamma_0}{2\hbar} \right] \underline{\mathbb{1}} + \underline{\tilde{W}}_{\vec{k}} + \frac{i}{\hbar} \underline{\epsilon} \right]^{-1} \right\}_{\alpha\beta} p_\beta. \quad (13)$$

The *a priori* probabilities p_β ($\beta=0,1$) are determined by the detailed balance with transition rates between the two isomer states:

$$W_0^{10} p_0 = W_0^{01} p_1, \quad p_0 + p_1 = 1.$$

With $W_0^{\alpha\beta}$ from Eq. (6) this yields

$$p_1 = 12c_v \frac{w_4}{w_3} p_0 = 12c_{NN} p_0 = \frac{12c_{NN}}{1 + 12c_{NN}}. \quad (14)$$

The inversion of the 2×2 matrix in Eq. (13) can be done explicitly and the emission probability can be written as a two-line spectrum

$$\sigma_e(\vec{k}, \omega) = f_v \frac{1}{2\pi\hbar} \text{Re} \left[\frac{A_1(\vec{k})}{z_1 - i\omega} + \frac{A_2(\vec{k})}{z_2 - i\omega} \right], \quad (15)$$

where the positions of the lines are determined by the zeros of the determinant

For the calculation of the emission probability, Eq. (2), we need the self-correlation function in the time-wave-vector domain

$$\begin{aligned} \underline{G}_D(\vec{k}, t) &= \int_{-\infty}^{+\infty} d\omega e^{-i\omega t} \underline{\tilde{G}}(\vec{k}, \omega) \\ &= \Theta(t) e^{-\underline{\tilde{W}}_{\vec{k}} t}. \end{aligned} \quad (10)$$

Here $\Theta(t) = 1$ for $t \geq 0$, and $\Theta(t) = 0$ for $t < 0$. Formula (10) shows that the eigenvalues of the Fourier transform of the transition matrix are the relaxation rates for the self-correlation function \underline{G}_D . It is given by

$$\underline{\tilde{W}}_{\vec{k}}^{\alpha\beta} = W_0^{\alpha\beta} + \delta_{\alpha 1} \delta_{\beta 1} w_2 [1 - s(\vec{k})] \quad (11)$$

with $W_0^{\alpha\beta}$ from Eq. (6) and

$$s(\vec{k}) = \frac{1}{Z} \sum_{\vec{R}^{\vec{n}}} e^{i\vec{k} \cdot \vec{R}^{\vec{n}}} \quad (12)$$

the form factor of the NN shell ($\vec{R}^{\vec{n}} \in \text{NN}$). For the fcc lattice it is given by

$$\begin{aligned} s^{\text{fcc}}(\vec{k}) &= \frac{1}{3} \left[\cos \left[\frac{a}{2} k_x \right] \cos \left[\frac{a}{2} k_y \right] \right. \\ &\quad + \cos \left[\frac{a}{2} k_y \right] \cos \left[\frac{a}{2} k_z \right] \\ &\quad \left. + \cos \left[\frac{a}{2} k_z \right] \cos \left[\frac{a}{2} k_x \right] \right] \end{aligned}$$

with a the lattice constant. Inserting Eq. (10) into Eq. (2) we obtain for the emission probability

$$D(z) = \det \left[\left[-z + \frac{\Gamma_0}{2\hbar} \right] \mathbb{1} + \tilde{W}_{\vec{k}} + \frac{i}{\hbar} \epsilon \right] = 0 \quad (16)$$

yielding

$$z_{1,2} = \frac{\Gamma_0}{2\hbar} + i \frac{\epsilon_0}{\hbar} + \frac{1}{2} \{ (i\delta_1 + \tilde{W}_{\vec{k}}^{11} + \tilde{W}_{\vec{k}}^{00}) \mp [(i\delta_1 + \tilde{W}_{\vec{k}}^{11} - \tilde{W}_{\vec{k}}^{00})^2 + 4\tilde{W}_{\vec{k}}^{10}\tilde{W}_{\vec{k}}^{01}]^{1/2} \} \quad (17)$$

with

$$\hbar\delta_1 = \epsilon_1 - \epsilon_0 \quad (18)$$

the isomer shift due to an associated vacancy. The relevant combinations of the transition rates are given by

$$\begin{aligned} \tilde{W}_{\vec{k}}^{11} + \tilde{W}_{\vec{k}}^{00} &= (1 + 12c_{\text{NN}})7w_3 + w_2[1 - s(\vec{k})], \\ \tilde{W}_{\vec{k}}^{11} - \tilde{W}_{\vec{k}}^{00} &= (1 - 12c_{\text{NN}})7w_3 + w_2[1 - s(\vec{k})], \quad \tilde{W}_{\vec{k}}^{10}\tilde{W}_{\vec{k}}^{01} = 12c_{\text{NN}}(7w_3)^2. \end{aligned} \quad (19)$$

The weights are given by

$$A_{1,2}(\vec{k}) = \pm (z_1 - z_2)^{-1} \left[z_{1,2} - \frac{\Gamma_0}{2\hbar} - i \frac{\epsilon_0}{\hbar} - \left((1 + 12c_{\text{NN}})7w_3 + \frac{w_2[1 + s(\vec{k})] + i\delta_1}{1 + 12c_{\text{NN}}} \right) \right] \quad (20)$$

The spectrum thus consists of two lines whose positions are given by the imaginary parts of $z_{1,2}$, the widths by the real parts of $z_{1,2}$, and the weights by $A_{1,2}$. All functions are determined by the concentration and jump frequencies of vacancies in the neighborhood of the MA, and by the isomer shift.

To be more specific, let us assume that the vacancy concentration is small even on the nearest-neighbor shell of the MA. Then we can expand $z_{1,2}$ and $A_{1,2}$ with respect to the small parameter $12c_{\text{NN}}$. This yields for the widths and positions of the lines

$$z_1 \simeq \frac{\Gamma_0}{2\hbar} + (12c_{\text{NN}})(7w_3)(1 - Q(\vec{k})\{7w_3 + w_2[1 - s(\vec{k})]\}) + i \left[\frac{\epsilon_0}{\hbar} + \delta_1(12c_{\text{NN}})(7w_3)Q(\vec{k}) \right], \quad (21a)$$

$$z_2 \simeq \frac{\Gamma_0}{2\hbar} + \{7w_3 + w_2[1 - s(\vec{k})]\}[1 + (12c_{\text{NN}})(7w_3)Q(\vec{k})] + i \left[\frac{\epsilon_1}{\hbar} - \delta_1(12c_{\text{NN}})(7w_3)Q(\vec{k}) \right], \quad (21b)$$

with

$$Q(\vec{k}) = 7w_3(\delta_1^2 + \{7w_3 + w_2[1 - s(\vec{k})]\}^2)^{-1}, \quad (21c)$$

and for the weights

$$A_1 = 1 - A_2, \quad (22)$$

$$A_2 \simeq 12c_{\text{NN}}(1 - Q(\vec{k})\{7w_3 + w_2[1 - s(\vec{k})] - i\delta_1\})^2.$$

In this limit the two lines describe the emission of the γ ray if the MA is or is not associated with a vacancy, respectively. The lines are asymmetric due to the imaginary part of $A_{1,2}$ which is proportional to $12c_{\text{NN}}Q(\vec{k})\delta_1$. This shows that the asymmetry is only relevant if δ_1 is of the same order of magnitude as the vacancy jump frequencies. Because the overlap is small the lines are essentially centered at the respective nuclear transition energy, ϵ_0 and ϵ_1 . For small vacancy concentrations each MA is in the nonassociated state most of the time and the no-

vacancy line carries almost all the intensity.

Also, the contributions to the linewidths due to diffusion are differing by orders of magnitudes: While the additional width of the no-vacancy line is proportional to the vacancy concentration c_{NN} the width of the vacancy line to first order does not depend on the vacancy concentration but is of the order of the vacancy jump frequencies. This can be understood because the rate of change of the nonassociated state is given by the association rate of vacancies to the NN shell which is proportional to the vacancy concentration whereas the changes within the associated state (exchange of sites of MA with vacancy, w_2) and out of this state (dissociation of vacancies, w_3) are governed by the local motion of an associated pair and thus the width is proportional to vacancy jump frequencies *directly*. This means that the vacancy line is broader by a factor of $(c_{\text{NN}})^{-1}$, and thus is hard to measure at high temperatures where the additional width of the no-vacancy line is of the order of the natural linewidth.

At lower temperatures the intensity of the vacancy line decreases rapidly proportional to c_{NN} and is thus invisible.

Only the no-vacancy line due to nonassociated MA whose width is caused by long-range migration of the MA is observed and we shall discuss this in detail now.

Experimentally it is found that the shift of the no-vacancy line caused by the overlap with the vacancy line [the term proportional to δ_1 in Eq. (21a)] is small compared to the diffusion-induced width which at high temperatures is of the order of the natural linewidth Γ_0 . This can be explained either by assuming

$$\delta_1 \gg (w_3, w_2) \simeq \text{Re}z_1 / c_{\text{NN}} \simeq \Gamma_0 / c_{\text{NN}}$$

which is unrealistically large or by $\delta_1 \ll (w_3, w_2)$. We shall assume the second case to be true and neglect δ_1 in the expression for z_1 .

The \vec{k} dependence, i.e., the anisotropy of the linewidth, depends strongly on the relation between the vacancy jump frequencies in the neighborhood of the MA. Most significant is the decrease of the width close to every reciprocal lattice point \vec{K} , where $s(\vec{k}) \rightarrow 1$. Then

$$\text{Re}z_1 \simeq \frac{\Gamma_0}{2\hbar} + 12c_{\text{NN}}w_2 \frac{d^2}{6} (\vec{k} - \vec{K})^2, \quad (23)$$

which means that the diffusion-induced width goes to zero proportional to the square of the distance to the reciprocal lattice vector. The proportionality factor is the diffusion coefficient of the MA:

$$D_{\text{MA}} = 12c_{\text{NN}}w_2 \frac{d^2}{6} \quad (24)$$

with d the NN distance. There is no correlation factor involved in this model since it is assumed that the rotation frequency w_1 is the largest vacancy jump frequency in the NN shell of the MA. (See previous discussion and Fig. 2.)

Far away from the reciprocal lattice vectors we can distinguish two limiting cases:

(i) $[1 - s(\vec{k})]w_2 \gg 7w_3$, i.e., a vacancy makes many jumps with the MA before it dissociates. Together with $w_1 \gg w_2$ this means that one vacancy can move the MA very far compared to the wavelength $2\pi/k$ of the γ rays. This results in a constant width of the line

$$\text{Re}z_1 \simeq \frac{\Gamma_0}{2\hbar} + (12c_{\text{NN}})(7w_3) \quad (25)$$

except close to reciprocal lattice points where $1 - s(\vec{k})$ goes to zero and the inequality (i) cannot be fulfilled.

(ii) $[1 - s(\vec{k})]w_2 \ll 7w_3$, i.e., a vacancy dissociates

quickly from the MA. The resulting narrow distribution yields a strongly anisotropic width over the entire Brillouin zone

$$\text{Re}z_1 \simeq \frac{\Gamma_0}{2\hbar} + 12c_{\text{NN}}w_2 [1 - s(\vec{k})]. \quad (26)$$

In this modified Krivoglaz model with $c_{\text{NN}} \ll 1$ the Mössbauer spectrum consists of two lines of which only one can be observed. Owing to the temperature-dependent vacancy concentration the intensity of the lines is temperature dependent [see Eq. (22)].

The main shortcoming of the model is the fact that correlations between the motion of a vacancy and a MA cannot be described. This is evident in the expression for the macroscopic diffusion coefficient, Eq. (24), which does not contain any correlation factor. Thus also the description of the anisotropy of the linewidth is limited to cases of uncorrelated diffusion.

B. The encounter model

For the full description of the linewidth of the no-vacancy line we use the encounter model with the assumption of instantaneous atom transfer.^{26,11,28} This assumption is justified as long as the duration of the encounter is short compared to the lifetime of the excited state. Owing to the neglect of the time dependence during an encounter this model can only yield *one line* whose width is determined by the long-range migration of the MA. This line corresponds to the no-vacancy line in the Krivoglaz model described above. One can show^{27,28} that in this model the linewidth is given by

$$\begin{aligned} \text{Re}z_1(\vec{k}) = & \Gamma_0 / 2\hbar + 12c_{\text{NN}}w_2 [z_{\text{enc}}(w_i)]^{-1} \\ & \times \left[1 - \sum_{\vec{n}} e^{i\vec{k} \cdot \vec{R}^{\vec{n}}} W_{\text{enc}}(\vec{R}^{\vec{n}}, w_i) \right]. \end{aligned} \quad (27)$$

Here Γ_0 , c_{NN} , and the jump frequencies w_i have the meaning defined above. $z_{\text{enc}}(w_i) = (1 - p_R)^{-1}$ is the mean number of MA jumps during an encounter with p_R the return probability of a vacancy from a NN site to the site of the MA,¹¹ and $W_{\text{enc}}(\vec{R}^{\vec{n}} - \vec{R}^{\vec{m}})$ is the probability that as a result of all jumps of the MA during an encounter the MA is displaced from site $\vec{R}^{\vec{m}}$ to site $\vec{R}^{\vec{n}}$. In Eq. (27) we have indicated the implicit dependence on the perturbed vacancy jump frequencies of z_{enc} and W_{enc} . The result for the linewidth is analogous to the result obtained for self-diffusion by Wolf.¹⁰

For the assumptions of the Krivoglaz model ($w_1 \gg w_2, w_3$) Eq. (27) reduces to Eqs. (23) and (26)

in the respective limiting cases. For general jump-frequency ratios, however, it includes correlation effects. The case of small dissociation frequency $w_3 \rightarrow 0$ leads to infinitely large z_{enc} . As discussed above Eq. (27) can only be applied if the duration of the encounter ($\sim w_3^{-1}$) is still short compared to the lifetime of the excited state (Γ_0^{-1}). Then the natural linewidth dominates as can be seen from Eqs. (25) and (27).

We have calculated the encounter parameters z_{enc} and W_{enc} within the five-frequency model using a modified version of a Monte Carlo program by Wolf and Differt.³⁰ In Table I and Fig. 3 the results for some values of the vacancy jump frequencies are shown. As expected we find the following features.

The encounter parameters z_{enc} and W_{enc} are most sensitive to the ratios w_1/w_3 and w_2/w_3 . These frequencies are in direct competition and they determine how often the MA exchanges sites with the vacancy. There is a minor dependence on the ratio w_4/w_0 of the association frequency w_4 to the ideal jump frequency w_0 which determines the return probability of a vacancy to the NN shell. W_{enc} and z_{enc} are independent of the fourth ratio w_4/w_3 and thus also of the parameter α of Table I. From the principle of detailed balance one can show that w_4/w_3 is proportional to the equilibrium concentration of vacancies, c_{NN} , and thus determines the absolute value of the line broadening.

For self-diffusion (model 1, all $w_i = w_0$) and for models with $(w_1, w_2) \ll w_3$ (model 5) the MA distribution is very narrow, i.e., more than 95% of all MA end up within the second-neighbor shell of the initial site because the return probability p_R is small. Thus the correlation factor f_{MA} is close to unity in accordance with earlier results.³¹ If w_2 and/or w_1 are larger than w_3 (models 2, 3, and 4) the MA distribution becomes wider because the return probability increases. For model 3, e.g., less than 55% of the impurity atoms end up within the second-neighbor shell.

In Fig. 4 we have plotted the angular dependence of the diffusional line broadening for values characterizing ^{57}Fe ($k = 72.98 \text{ nm}^{-1}$) in an Al single crystal at 923 K ($a = 0.413 \text{ nm}$). As can be seen, narrow

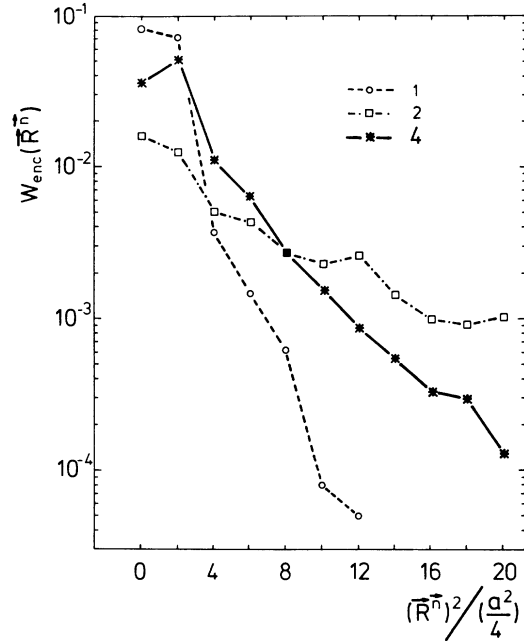


FIG. 3. Final distribution of Mössbauer atom after encounter with vacancy $W_{\text{enc}}(\vec{R}^n)$ vs $(\vec{R}^n)^2$. Note the logarithmic scale. The model numbers refer to Table I.

distributions of W_{enc} lead to highly structured linewidths, for wider distributions the structure becomes less pronounced. This is easily understood if one considers that the anisotropy of the diffusional broadening is due to an interference of the γ wave between the initial site and the final site of the encounter. The larger the number of different final sites the weaker the anisotropy.

The persisting structure can be explained using the reciprocal lattice plot, Fig. 5, with the Ewald sphere of radius k_{Fe} of the ^{57}Fe Mössbauer transition. As discussed before, for diffusion on a discrete lattice the linewidth $\text{Re}z_1(\vec{k})$ is a periodic function of \vec{k} . This means that the diffusion-induced broadening tends to zero close to every reciprocal lattice point³²:

$$\text{Re}z_1(\vec{k}) = \frac{\Gamma_0}{2\hbar} + D_{\text{MA}}(\vec{k} - \vec{K})^2, \quad \vec{k} \rightarrow \vec{K}. \quad (28a)$$

TABLE I. Parameters for encounters in fcc crystals.

No.	w_i/w_0				f_{MA}	z_{enc}	$\vec{R}^n = \vec{0} = (000)$	$10^5 W_{\text{enc}}(\vec{R}^n)$					Sum of all $\vec{R}^n \geq (222)$
	1	2	3	4				(110)	(200)	(211)	(220)	(310)	
1	α	α	α	1	0.7815	1.3447	8178	7083	365	149	62	8	124
2	α	α	0.01α	1	0.5357	33.357	1600	1233	500	433	275	229	61 400
3	10α	α	0.1α	1	0.9051	4.119	3400	3600	1300	654	383	279	18 600
4	15α	α	0.1α	0.02	0.9302	2.451	3700	4833	1133	629	350	171	7500
5	0.1α	0.1α	α	1	0.9529	1.04	2200	8075	83	17	0	0	0

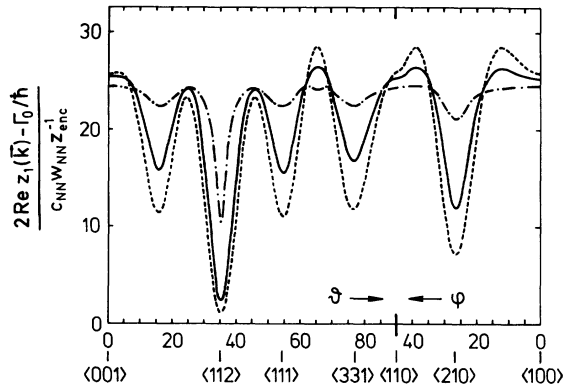


FIG. 4. Relative anisotropy of Mössbauer linewidth for Fe in Al single crystal vs emission angle. Models are designated by the same line symbols as in Fig. 3.

Different from the Krivoglaz model, in the encounter model correlation effects are included and the diffusion coefficient reads

$$D_{MA} = 12c_{NN}w_2 \frac{d^2}{6} f_{MA}(w_i), \quad (28b)$$

where the macroscopic correlation factor f_{MA} is determined by the ratios of the vacancy jump frequencies.³¹ It can approximately be written as

$$f_{MA} \approx \frac{w_1 + \frac{7}{2}w_3}{w_1 + w_2 + \frac{7}{2}w_3}, \quad (29)$$

which shows that for $w_1 \gg (w_2, w_3)$ (Krivoglaz model) $f_{MA} \approx 1$, which means no correlation.

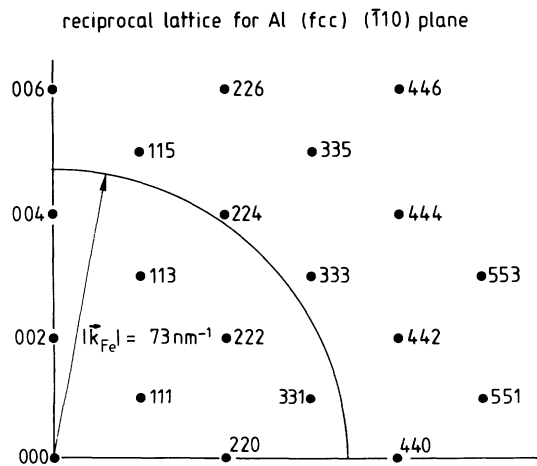


FIG. 5. Ewald sphere for \vec{k} vector of Fe-Mössbauer line in Al reciprocal lattice. Whenever the sphere is close to a reciprocal lattice point a minimum of the linewidth is expected (see Fig. 4).

Figure 4 shows that the minima of $z_1(\vec{k})$ can all be related to directions where the Ewald sphere comes close to a reciprocal lattice point of Al. This is particularly true for $\langle 112 \rangle$ direction which shows the most pronounced minimum for all models.

C. Discussion

From these theoretical results we conclude that three experimental features of the Mössbauer spectrum can be used to obtain information about the interaction of vacancies with Fe impurities in Al:

(i) According to Eq. (22) one can use the temperature dependence of the intensity of the no-vacancy line to determine the vacancy concentration on NN sites and thus the Fe-vacancy binding energy.

(ii) The temperature dependence of the linewidth, particularly close to the $\langle 112 \rangle$ direction, can be used directly to determine the activation energy for Fe diffusion in Al.

(iii) As can be seen from Fig. 4 one can use the variation of the anisotropy of the linewidth to find relations between the vacancy jump frequencies in the NN shell of the MA. Of course, the choice of the parameters is limited by results of other experiments. For example, the absolute value of the diffusion-induced Mössbauer line broadening has to be consistent with the Fe diffusion coefficient measured by the tracer technique^{33,34} and the relation between the Fe diffusion coefficient and the self-diffusion coefficient³⁵ has to be fulfilled.

III. EXPERIMENTAL

A. Source preparation

The solid solubility of Co in Al (Ref. 36) is very small, close to the melting point about 0.01 at.% Co atoms can be solved at substitutional lattice sites.^{37,38} The corresponding equilibrium concentration of Co at room temperature is far below 0.1 ppm, thus, fast quenching from high temperatures becomes necessary to obtain reasonably strong single-line Mössbauer sources.

From a 99.9999% Al single crystal, disks with dimensions of $1.1 \times 0.7 \times 0.1 \text{ cm}^3$ were spark cut with faces parallel to the (111) plane. These wafers were etched with a solution of 25% H_2SO_4 , 5% HNO_3 , 70% H_3PO_4 at 355 K to a thickness of about 300 μm . About 18 mCi carrier-free $^{57}\text{CoCl}_2$ solved in 0.1 M hydrochlorid acid solution were used for doping. After eliminating HCl by freeze-drying the $^{57}\text{CoCl}_2$ salt was solved in $\approx 1 \text{ ml}$ high-purity distilled water. In a glove box with pure He atmosphere 10- μl drops of the liquid were spread over the surface of the crystal in order to achieve a homo-

geneous concentration of $^{57}\text{CoCl}_2$. After drying, the crystal was placed on an Al_2O_3 disk in a vacuum-tight quartz tube and then Cl was reduced at 573 K in a flowing He- H_2 gas mixture for 4 h. ^{57}Co was diffused into the crystal at 928 K in flowing He gas for 7 d. Rapid quenching into pure water at room temperature finished the doping.

Mössbauer spectra of the quenched crystals showed that part of the ^{57}Co are solved at substitutional lattice sites, part have trapped vacancies, and part of the Co atoms were hindered to diffuse into the bulk by a surface barrier. Such a hold-up effect of the Co atoms at a surface layer is reported in the literature.^{33,39} Following annealing of quenched-in vacancies at ≈ 473 K and removing a surface layer by etching we observed Mössbauer spectra with only one resonance with full width at half maximum (FWHM) of 0.235 mm/s and an isomer shift of -0.425 mm/s (with respect to a natural iron absorber) at room temperature. Most probably these values correspond to solid substitutional sites of ^{57}Fe in Al.^{40,41} Homogeneous distribution of the ^{57}Co was shown by autoradiography. γ diffractometry proved low mosaic spread of the single crystal before and after the diffusion treatment [FWHM of the (220) reflection ≈ 15 min]. The final concentration of ^{57}Co in the single crystal was about 10 ppm.

B. High-temperature technique

The high-temperature measurements were performed in an ultrahigh-vacuum sample chamber in which a furnace with three individually controlled sections was installed. The middle section of the furnace had a slit over 180° parallel to the horizontal plane for the detection of the γ radiation. The radiation window of the sample chamber was made by a $75\text{-}\mu\text{m}$ -thick polyimide foil with the absorption edge below 6 keV. A thermal radiation shield around the sample holder with a small slit for the γ radiation was used to minimize temperature gradients. Thermocouples in the three zones of the furnace were applied for temperature recording. The chromel-alumel thermocouples were calibrated before and after the high-temperature experiments at the solidus temperature of Al. The drifts due to aging of the thermocouples were less than 2 K over a period of 10 months. The temperature differences between the sample and the thermocouple were determined by melting and freezing a dummy specimen. The temperature distribution in time never drifted more than ± 0.15 K during 24 h. However, during the complete time of the measurements of the anisotropy of the diffusional broadening of the Mössbauer resonance a total temperature deviation of ≤ 2 K was observed mainly due to aging of the

thermocouples as mentioned above. Such a variation in temperature causes a change in the Mössbauer linewidth of about < 0.002 mm/s which is much less than the experimental error in the determination of the half width (± 0.015 mm/s) for the high-temperature measurements. All the measurements were carried out in a vacuum of 3×10^{-6} mbar. In order to prevent vibrations a sputter ion pump was used and the whole experimental setup was placed on an antivibration support. The furnace was heated by dc to avoid noise on the thermocouples and on the Mössbauer drives.

The Al single crystal was placed on a pure Al foil and mounted on a stainless steel source holder. The specimen was oriented on the holder by Laue diffraction such that the $\langle 100 \rangle$, $\langle 111 \rangle$, and $\langle 110 \rangle$ directions were parallel to the horizontal 180° slit in the sample chamber.

C. Mössbauer techniques

The measurements were performed with two identical spectrometers, each could be aligned in various directions with respect to the Al single crystal. The transmission spectrometers consisted of Mössbauer drives moving Pd-2 at.% ^{57}Fe absorbers (at room temperature) and of Kr gas proportional counters. The 14.4-keV γ rays and the counts of the escape peak were accumulated by an or-gate.

The FWHM of the Mössbauer resonance of the single crystalline Al $^{57}\text{Co}/^{57}\text{Fe}$ source measured with a Pd-2 at.% Fe absorber was 0.33 mm/s, the central shift was -0.26 mm/s at room temperature. The convention of positive velocity for approaching relative motion between source and absorber is adopted, thus an increase in the electron density at the source nucleus gives rise to a positive change in the isomer shift.

Lead collimators of rectangular shape were used to define the angular resolution of the Mössbauer spectrometers. The angular resolution function $R(\vartheta, \varphi)$ had the shape of a trapezoid, with areas of $0.8^\circ \times 5^\circ$ at the top and of $8^\circ \times 11.4^\circ$ at the base. In order to compare the experimental results with model calculations of the anisotropic diffusional broadening of the Mössbauer resonance the theoretical curves had to be folded with the angular resolution function.

IV. RESULTS AND DISCUSSION

A. Mössbauer spectra and their interpretation

Figure 6 shows Mössbauer spectra for ^{57}Fe in Al: spectra measured at 923 K (11 K below the melting point of the sample) exhibit a broadened single line

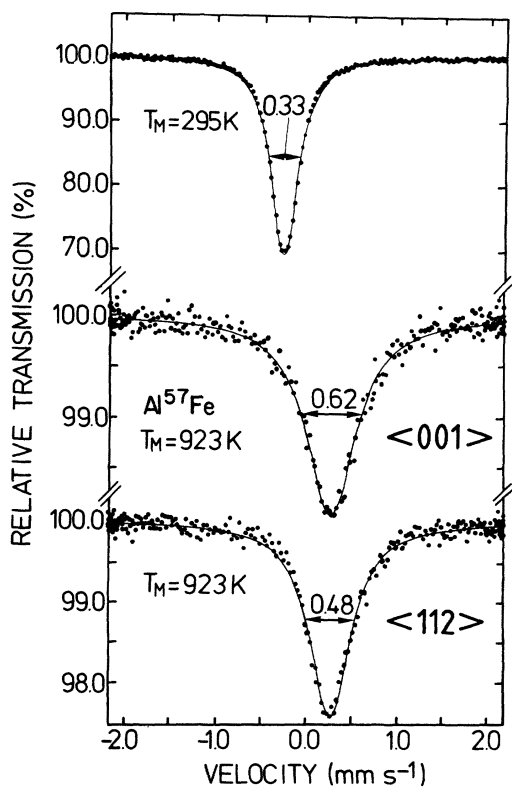


FIG. 6. Mössbauer spectra of ^{57}Fe in Al at 923 K for different orientations, and at 295 K. Central shifts are relative to a Pd 2 at.% ^{57}Fe absorber at RT. Notice that the diffusional broadening is larger in the $\langle 001 \rangle$ than in the $\langle 112 \rangle$ direction.

compared to spectra measured at room temperature (RT). In addition, the figure shows that this increase in the linewidth is different for different directions of observation relative to the single-crystal axes as is expected for diffusive motion of the Fe atoms.

The position of the resonance as a function of temperature is given in Fig. 7. In a Mössbauer experiment the shift of the nuclear resonance from zero energy difference between source and absorber (zero Doppler velocity) is primarily due to the isomer shift. This is a measure for the electron density at the ^{57}Fe nucleus, and thus contains information on the atomic structure in the neighborhood of the Mössbauer atom, e.g., about defects in the impurity's first-neighbor shell (see, e.g., Ref. 41). The temperature dependence of the shift is caused by the second-order Doppler effect (see, e.g., Ref. 42).

Below 870 K the Mössbauer spectra consist of several resonances. The reason is that besides the resonance from ^{57}Co - ^{57}Fe in solid solution in Al, resonances from intermetallic compounds of Al with

Co-Fe appear because the Co concentration in Al in our sample (~ 10 ppm) exceeds the solid solubility below 870 K. Data in this temperature range down to about 500 K have been determined from a fit of the Mössbauer spectrum with several components. By rapid quenching from temperatures above 870 K to temperatures below 500 K it is possible to freeze in the high-temperature conditions. That explains that spectra measured below 500 K again consist of a single line only (e.g., Fig. 6, the spectrum measured at RT).

The straight line through the points in Fig. 7 has a slope of $7.32 \times 10^{-4} \text{ mm/s}^{-1} \text{ K}^{-1}$ as given by the Dulong-Petit rule for the heat capacity.⁴² From the good fit of the data points with the Dulong-Petit rule we conclude that the high-temperature resonance is identical with the single line found at low temperatures in highly dilute samples which is attributed to ^{57}Fe atoms on substitutional sites in Al. Notice, however, that at RT we are far away from thermal equilibrium conditions. It is known from quenching²³ experiments that this line is a no-vacancy line, i.e., it is due to ^{57}Fe atoms without vacancies in their nearest neighborhood.

In principle one would expect to find a second line with a different isomer shift corresponding to an ^{57}Fe atom in the vacancy associated state (vacancy line).^{23,43} The absence of this line can be explained in the framework of the Krivoglaz model: According to Eq. (22) the intensity of the vacancy line is rather weak as long as c_{NN} is small. Close to the melting point where c_{NN} may be appreciably large the linewidth of the vacancy line [Eq. (21)] is of the order of the vacancy jump frequencies ω_2, ω_3 , i.e., it is considerably broader than the no-vacancy line. Consequently the vacancy line cannot be discriminated from the statistical fluctuations of the background.

At high temperatures the central shift (sum of isomer and second-order Doppler shift) of the no-vacancy line shows only a small deviation from the Dulong-Petit rule. This confirms the assumption of Sec. II A that the shift of the no-vacancy line caused by the overlap with the vacancy line is small in comparison to the natural linewidth Γ_0 .

B. Temperature dependence of the resonance intensity

Figure 8 shows the temperature dependence of the total resonance area F measured from room temperature (RT) up to temperatures close to the melting point, normalized to unity at RT. According to Sec. II, the area of the Mössbauer resonance is determined by the dynamics of the Mössbauer atom. If the jump rate of the MA due to diffusion is small the temperature dependence of the area is deter-

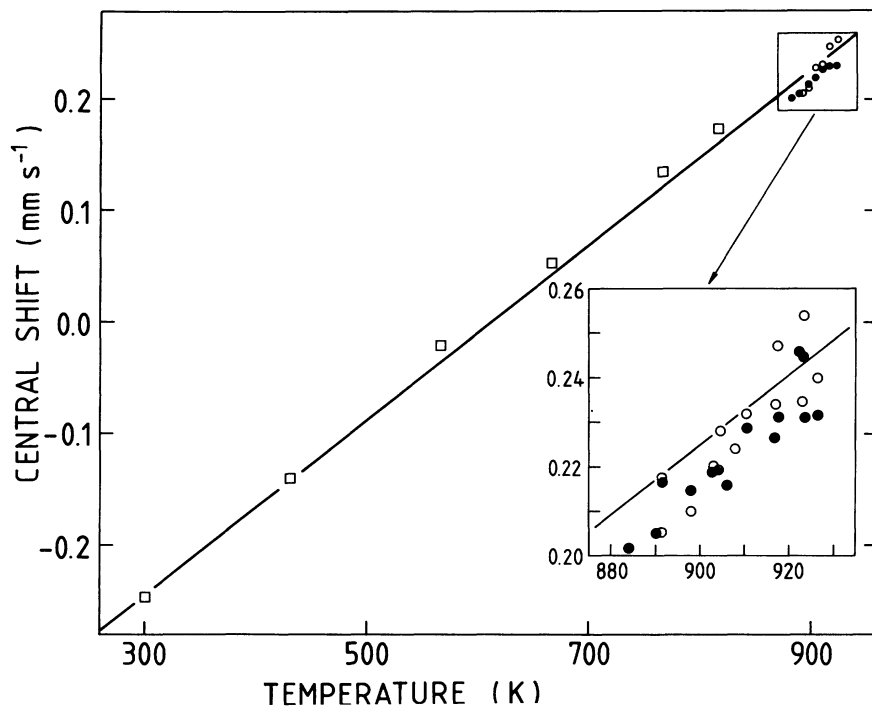


FIG. 7. Central shift (sum of isomer and second-order Doppler shift) of ^{57}Fe in Al vs temperature. \circ , $\langle 110 \rangle$ direction; \bullet , $\langle 112 \rangle$ direction; \square Al single crystal with smaller ^{57}Co - ^{57}Fe concentration (0.5 at. ppm). The straight line represents the slope given by the Dulong-Petit rule for the heat capacity.

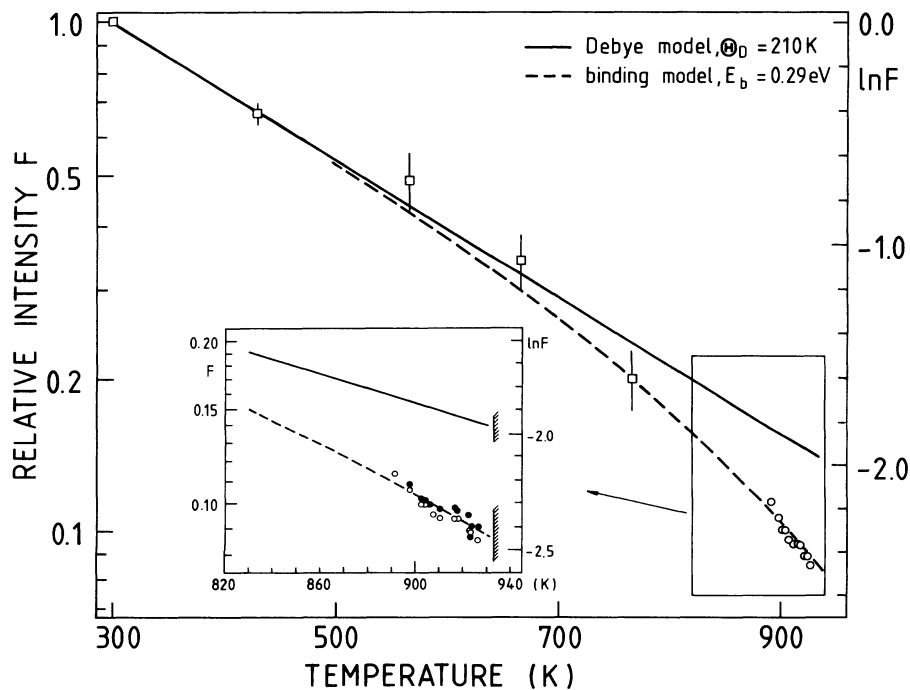


FIG. 8. Temperature dependence of the relative intensity F of the Mössbauer resonance of ^{57}Fe in an Al single crystal. Measurements are designated by the same symbols as in Fig. 7.

mined by the Debye-Waller factor f_v for vibrations. For Debye-type behavior at sufficiently high temperatures

$$f_v(T) = \exp \left[-\frac{6E_R}{k_B \Theta_D^2} T \right]. \quad (30)$$

Here E_R is the recoil energy from the emission of the γ quantum (1.95×10^{-3} eV for the 14.4-keV transition of ^{57}Fe), k_B is Boltzmann's constant, and Θ_D the Debye temperature.

Below 700 K the temperature dependence of the area of the no-vacancy resonance can be fitted by a Debye model with the Debye temperature $\Theta_D = 210$ K.¹⁵ Above 800 K, however, the resonance area decays much faster than would be expected from the Debye model. It is evident that vibrations alone cannot be responsible for this drastic decay.

As discussed in Sec. II, the intensity F of the no-vacancy resonance should decrease with increasing probability of vacancy association to an Fe impurity atom. The fractional area F corrected for the temperature dependence of the Debye-Waller factor should then follow the probability that a Mössbauer atom stays without a vacancy [Eq. (22)]

$$F(T) = \frac{f_v(T)}{f_v(\text{RT})} (1 - 12c_{\text{NN}}) = \frac{f_v(T)}{f_v(\text{RT})} A_1 \quad (31)$$

with the vacancy concentration c_{NN} at an NN site given by Eq. (7). Fitting the high-temperature data in Fig. 8 by Eq. (31) with $\Theta_D = 210$ K and $c_v(T)$ taken from literature^{44,45} (e.g., $c_v \simeq 8.2 \times 10^{-4}$ at 923 K) yields

$$E_b = 0.29 \pm 0.02 \text{ eV}.$$

Inserting this value in Eq. (7) yields the ratio of the dissociation to association jumps of a vacancy to the impurity NN shell

$$w_4/w_3 = 38$$

at 923 K.

C. Diffusional line broadening

Figure 9 shows the experimental data of the diffusional broadening of the Mössbauer resonance as a function of the direction of observation relative to the single crystal. Δ_{LW} denotes the difference of the

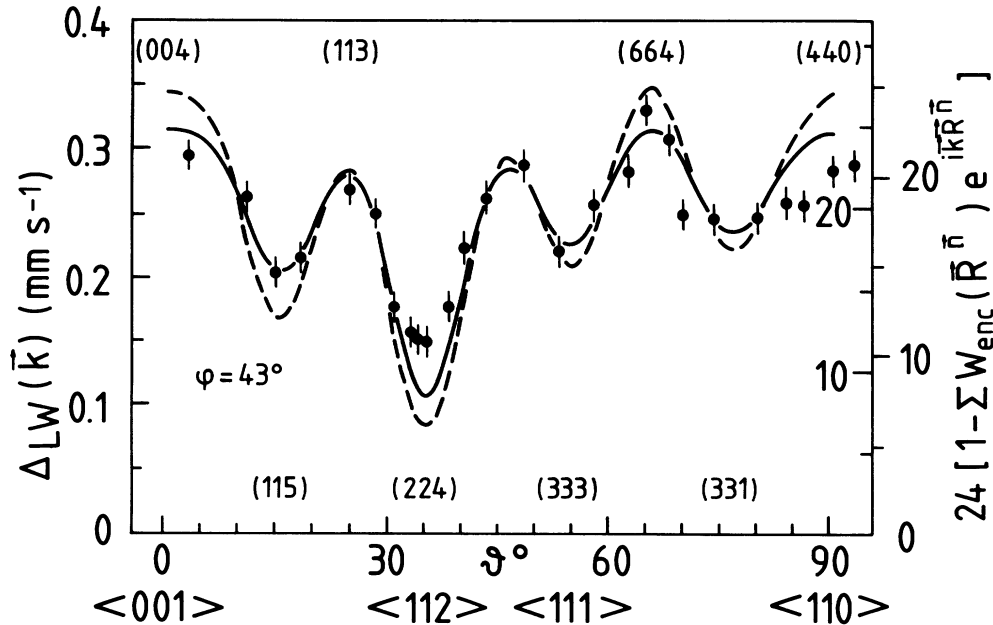


FIG. 9. Diffusional broadening Δ_{LW} of the Mössbauer resonance for ^{57}Fe in Al at 923 K as a function of observation direction. ϑ = polar angle, φ = azimuthal angle. Broken line and outer right scale: calculated anisotropy

$$[2 \text{Re} z_1(\vec{k}) - \Gamma_0 / \hbar] / (w_2 c_{\text{NN}} z_{\text{enc}}^{-1}) = 12 \times 2 \left[1 - \sum_n W_{\text{enc}}(\vec{R}_n) e^{i \vec{k} \cdot \vec{R}_n} \right]$$

for self-diffusion, solid line and inner right scale: calculation for impurity diffusion with frequencies as given in Table III. Calculations are folded with experimental resolution.

TABLE II. Diffusion coefficients.

	D_0 (cm ² /s)	Q (eV)	D (923 K) (cm ² /s)	D_{MA}/D_{SD} (923 K)	Authors
Al self-diffusion	1.71	1.47	1.22×10^{-8}		Lundy and Murdock (Ref. 58)
		1.25			Fradin and Rowland (Ref. 59)
		1.28			Seeger <i>et al.</i> ^a (Ref. 35)
Fe in Al	9.1×10^5 135	2.68	2.11×10^{-9}	0.17	Hood (Ref. 33)
		2.00	1.67×10^{-9}	0.14	Alexander and Slifkin (Ref. 34)
		2.5			Sayed and Kovacs (Ref. 60)
		2.59			Tonejc (Ref. 61)
	0.12	1.4	2.09×10^{-9}		Sørensen and Trumphy (Ref. 15)
	$1.1 \times 10^{4 \pm 1}$	2.3 ± 0.2	2.89×10^{-9}	0.24	This work

^aSeeger *et al.* analyzed all data concerning self-diffusion in Al in the framework of mono- and divacancy contributions. Q gives the activation energy for monovacancy diffusion, D (923 K) includes both processes and was used for the calculation of D_{MA}/D_{SD} .

linewidth (in mm/s) measured at 923 K and at RT. The polar angle ϑ was varied, and the azimuthal angle was kept constant at $\varphi=43^\circ$ for all measurements. The crystal orientations given in the figure correspond to $\varphi=45^\circ$, i.e., the 2° deviation of φ was ignored here but will be taken into account in the following model calculations.

The broken line corresponds to the self-diffusion model for NN jumps in the fcc Al lattice (model 1 in Table I and Fig. 4) as outlined in Sec. II B, but now folded with the experimental resolution. In this model all jump frequencies w_i are equal and correlation is a purely geometrical phenomenon. The experimentally measured minima and maxima of the line broadening are exactly where expected for $\langle 110 \rangle$ NN jumps in an fcc lattice. This proves that the Fe atoms are diffusing as substitutional impurities in Al, mostly by jumps to NN vacancies. As illustrated by the Ewald construction (see Fig. 5) the positions and the heights of the extrema are sensitive to small changes of the diffusion lattice. With the given experimental resolution we would have seen about a 4% change of the jump distance. Thus the figure shows that non-NN jumps as proposed by Janot⁴⁶ can only make minor contributions to the diffusion of Fe in Al.

Using the self-diffusion (SD) model we can determine an effective jump frequency for the MA-vacancy jump by adjusting the absolute value of the

measured diffusion broadening to the calculated curve. This yields $w'_0 = 1.67 \times 10^9 \text{ s}^{-1}$ at 923 K which is about 15% of $w_0 = 1.11 \times 10^{10} \text{ s}^{-1}$ for self-diffusion in Al.³⁵ The ratio w'_0/w_0 agrees well with the ratio of the diffusion coefficients D_{MA}/D_{SD} measured by tracer technique (compare Table II).

However, this modified self-diffusion model is not correct as can be seen from the difference between theoretical and experimental anisotropy. In addition, we have determined a binding between Fe atoms and vacancies. Consequently, we have to take into account more than one jump frequency to describe the Fe diffusion microscopically, as is well known from the work of Le Claire.³ The perturbation of the vacancy jump frequencies shows up in the smoothening of anisotropy of the line broadening $\Delta_{LW}(\vec{k})$ relative to the theoretical curve for self-diffusion. As shown in Sec. II B the anisotropy will be less pronounced for broader distributions $W_{enc}(\vec{R}^{\vec{n}})$, i.e., if more jumps occur during one encounter. In order to vary $W_{enc}(\vec{R}^{\vec{n}})$ and in this way find a fit for the measured anisotropy in the framework of the five-frequency model we have to allow different w_i and insert them into Eq. (27). The solid line in Fig. 9 represents the best fit, the corresponding values for $w_1, w_2, w_3, w_4, z_{enc}$, and f_{MA} are given in Table III.

The following remarks should be made.

(a) From the smoothening of the anisotropy it fol-

TABLE III. Vacancy jump frequencies for the diffusion of Fe in Al at 923 K. The ratios $w_1:w_2:w_3$ are determined from the fit of the experimentally measured *anisotropy* of the line broadening. Their absolute values, however, are determined from the *absolute value* of the line broadening and the ratio w_4/w_3 is determined in Sec. IV B. w_0 has been calculated from self-diffusion data (e.g., Ref. 35).

w_0	w_1	w_2	w_3	w_4	f_{MA}	z_{enc}
$1.1 \times 10^{10} \text{ s}^{-1}$	$1.3 \times 10^{9 \pm 0.5} \text{ s}^{-1}$	$6 \times 10^{7 \pm 0.5} \text{ s}^{-1}$	$8 \times 10^{6 \pm 0.5} \text{ s}^{-1}$	$3 \times 10^{8 \pm 0.5} \text{ s}^{-1}$	0.92	1.98

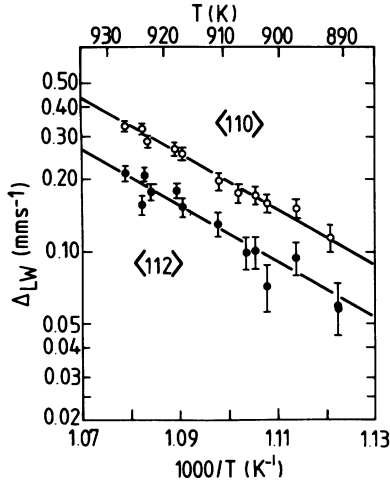


FIG. 10. Temperature dependence of the diffusional line broadening for ^{57}Fe in an Al single crystal for two different observation directions.

lows that both w_1, w_2 are larger than w_3 . Physically this means that the anisotropy of the no-vacancy line is less pronounced (smoothened) since more jumps occur during one encounter. Satisfactory fits are obtained for w_1 2 orders of magnitude larger than w_3 . Thus, the principal assumption of the Krivoglaz model $w_1 \gg w_2, w_3$ is fulfilled. Therefore, the vacancy line is practically undetectable and it is permitted to focus the attention on the no-vacancy line as has been done in the encounter model. The value of w_2 is such that we are between the two limiting cases of Eqs. (25) and (26). This means that the line broadening is proportional to $c_{\text{NN}} = c_v w_4 / w_3$ times a factor between $7w_3$ and $w_2[1-s(k)]$.

(b) The frequency set is very similar to the frequencies used in model 4 of Fig. 3 and Table I. In comparison to the self-diffusion model the distribution $W_{\text{enc}}(\vec{R}^{\vec{n}})$ of the MA after an encounter is decreased for the NN and next NN shell, but increased by orders of magnitude for all more distant shells.

Figure 10 shows the temperature dependence of Δ_{LW} for two different directions of observation relative to the single crystal, namely for the $\langle 112 \rangle$ direction where Δ_{LW} exhibits the most pronounced minimum (here $\vec{k} \rightarrow \vec{K}$) and for the $\langle 110 \rangle$ direction where Δ_{LW} shows a relative maximum.⁴⁷ It is obvious that within the accuracy of the measurements the temperature dependence is the same in both directions. This implies that the anisotropy does not change in the temperature range investigated which indicates that the diffusion mechanism does not change.

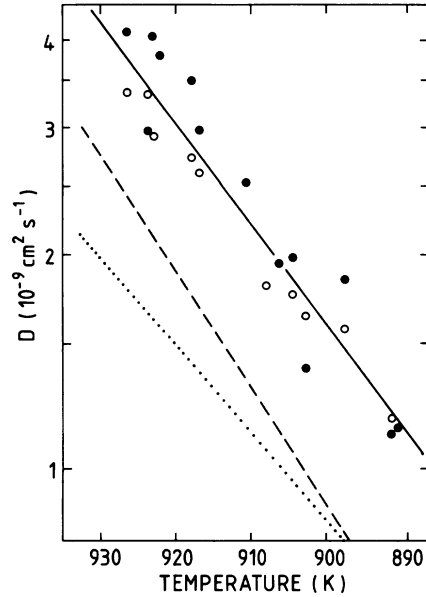


FIG. 11. Diffusion coefficient for Fe in Al: \circ , $\langle 110 \rangle$; \bullet , $\langle 112 \rangle$; and —, present result; — — —, Hood (Ref. 33); \cdots , Alexander and Slifkin (Ref. 34).

We can now use the known anisotropy which yields z_{enc} , f_{MA} , and W_{enc} to determine the diffusion coefficient from the measured temperature dependence of the line broadening in *one* direction. According to Eqs. (27) and (28b)

$$D_{\text{MA}}(T) = \frac{[2 \text{Re}z_1(\vec{k}, T) - \Gamma_0/\hbar] z_{\text{enc}} d^2 f_{\text{MA}}}{12 \left[1 - \sum_n e^{i\vec{k} \cdot \vec{R}^{\vec{n}}} W_{\text{enc}}(\vec{R}^{\vec{n}}) \right]} \quad (32)$$

$2 \text{Re}z_1(\vec{k}, T) - \Gamma_0/\hbar$ is connected to the experimentally determined line broadening $\Delta_{LW}(\vec{k}, T)$ measured in mm/s by

$$2 \text{Re}z_1(\vec{k}, T) - \Gamma_0/\hbar = \Delta_{LW}(\vec{k}, T) |\vec{k}| \quad (33)$$

We can determine $D_{\text{MA}}(T)$ separately for the two \vec{k} values by inserting $\Delta_{LW}(\vec{k}, T)$ and the corresponding structure factors (which are known from Fig. 9) into Eq. (32). Figure 11 shows the resulting Arrhenius plot of the diffusion coefficient. A least-squares fit with $D_{\text{MA}} = D_0 e^{-Q_{\text{MA}}/k_B T}$ where Q_{MA} is the activation energy for diffusion of the Mössbauer atom gives

$$D_{\text{MA}} = 1.1 \times 10^{4 \pm 1} e^{(2.3 \pm 0.2 \text{ eV})/k_B T} \text{ cm}^2/\text{s}.$$

Whereas the activation energy depends only on the *slope* of the diffusion broadening, i.e., Q_{MA} is already given by the slopes of Fig. 10, the prefactor is

sensitive to errors due to an inaccurate determination of the structure factor. In comparison to the activation energy for Al self-diffusion (Table II) the activation energy for Fe diffusion is surprisingly high. We shall discuss this in Sec. IV E.

As discussed in Sec. II B one can determine the diffusion coefficient from the diffusional broadening close to a reciprocal lattice vector without reference to the details of the anisotropy. In our case this would be possible in the $\langle 112 \rangle$ direction. However, we have not done this because the experimental resolution was not sufficient to satisfy the condition ($\vec{k} \rightarrow \vec{K}^{(112)}$) for Eq. (28a) to hold.

In the framework of the five-frequency model it is possible to calculate the activation energy E_2 for the exchange jumps, supposed f_{MA} is temperature independent¹¹:

$$E_2 = Q_{MA} - Q_{SD} + E_m + E_b. \quad (34)$$

Inserting for $Q_{SD} = 1.28$ eV,³⁵ $E_m = 0.63$ eV,³⁵ $E_b = 0.29$ eV, and $Q_{MA} = 2.3$ eV as determined above one gets $E_2 = 1.94$ eV. Using these values and the ratio $w_2/w_0 = 5.45 \times 10^{-3}$ at 923 K (see Table III) yields an unexpectedly high value for the temperature-independent prefactor $(w_2/w_0)_0 = 7.63 \times 10^4$, which also shows up in the diffusion coefficient. For a verification (or falsification) of our model one has to perform the full analysis with data for the anisotropy of the linewidth obtained at different temperatures.

D. Possible contribution of divacancies to the diffusion

A smoothening of the anisotropy in the line broadening is also expected if the diffusion proceeds via more complex mechanisms than NN jumps via monovacancies, e.g., impurity jumps to more distant neighbors or diffusion via divacancies. Both mechanisms can contribute to a wider distribution $\mathcal{W}_{enc}(\vec{R}^n)$ and thus to a reduction of the anisotropy of the linewidth. There are no quantitative calculations for the contributions of non-NN jumps and we will not discuss this mechanism further. Quantitative calculations of $\mathcal{W}_{enc}(\vec{R}^n)$ for an impurity diffusion via divacancies are virtually impossible, because too many free parameters are involved (the relative contribution of divacancies, the various jump frequencies). But it is possible to calculate the line broadening for the self-diffusion mechanism using the encounter parameters calculated by Wolf.⁴⁸ The resulting reduction of the anisotropy of the linewidth is too small to fit the experimental curve in Fig. 9, in particular the ratio between the maximum width close to the $\langle 322 \rangle$ direction and

the minimum close to the $\langle 112 \rangle$ direction is only reduced by 18% if the diffusion proceeds by divacancies exclusively. This means that also for the divacancy mechanism extreme jump frequencies similar to those obtained for the monovacancy mechanism (particularly binding) would be necessary to explain the experimental results. As has been noted by Mehrer⁴⁹ binding of divacancies decreases the contribution of these defects to the long-range migration of impurities.

On the other hand, the evidence for a large divacancy contribution to Fe diffusion in Al from other experiments is inconclusive. Arrhenius plots for Fe diffusion in Al are straight within experimental errors.^{33,34} This holds also for seven other tracers in Al over a temperature range for which a divacancy analysis would suggest curvature.⁵⁰ However, Berger *et al.*^{1,51} interpret resistivity annealing in quenched Al with 7 ppm Fe in terms of trapped divacancies. Conclusions drawn from post-quench annealing studies to the thermal equilibrium state may be in error because a large divacancy population can be built up during the quench (quench rate $\sim 10^3$ deg/s) even if at the quench temperature only a few percent of the vacancies are in the form of divacancies.⁵²

In summary, our results do not support a large divacancy contribution to the long-range diffusion of Fe in Al, but it cannot be ruled out.

E. Comparison with literature

An anomalous decrease of the resonance area due to diffusion has already been observed in the early work of Knauer and Mullen on Cu ⁵⁷Fe and Au ⁵⁷Fe alloys⁵³ and later on in experiments on ⁵⁷Fe diffusion in Fe O_x.^{54,55} The authors attributed the deviation from a Debye-type behavior quite generally to anharmonic vibrations of the Mössbauer atom close to the melting point. On the contrary, we have attributed the entire anomalous temperature dependence of the intensity to binding effects, yielding $E_b = 0.29$ eV. Unfortunately, there is no direct measurement of the anharmonic change of the vibrational spectrum at temperatures close to the melting point even in pure Al,⁵⁶ so one can only speculate on the magnitude of anharmonic effects for Fe in Al. If there were an appreciable contribution to the anomalous decrease of the intensity the value for the binding energy would decrease. Thus our value is an upper limit for E_b . As a consequence the ratios $w_1:w_2:w_3$ are not affected, but the absolute values of these frequencies would increase keeping $c_{NN} \cdot w_2$ constant.

A comparison of the vacancy-Fe binding energy

$E_b \leq 0.29$ eV with values taken from the literature is problematic due to the lack of other experiments which measure the binding energy at thermal equilibrium conditions at high temperatures. From quenching^{23,51} experiments on Al/Fe samples the trapping of vacancies at the Fe atom is known. Perry and Entwistle⁵⁷ measured the effect of small concentrations of Fe atoms on the initial rate of clustering of Cu atoms in quenched AlCu alloys and obtained $E_b = 0.18$ eV. As discussed in Sec. IV D divacancies or larger vacancy clusters may be involved thus a *quantitative* comparison of this value with the larger binding energy estimated from the present work is not possible.

Previous experiments at Al/Fe alloys yielded differing diffusion coefficients (Table II). This is not surprising because these experiments are extremely difficult due to the low solubility of Fe in Al, to the competition of grain boundary diffusion or other short-circuiting mechanisms and to the unavoidable oxide barrier at the surface of the Al samples. This holds true also for the diffusion of other impurities in Al as Cr, Mn, Co, Ni, etc. (For a recent compilation see Ref. 38.) The present Mössbauer experiment avoids most of these experimental problems. All measurements were performed with the same single crystal at thermal equilibrium conditions (no grain boundaries, low dislocation density). Furthermore, the existence of one-line spectra showed that all Fe atoms were in solid solution and surface effects are of less importance because most of the measured γ quanta are emitted from ⁵⁷Fe atoms sitting in the bulk material. As shown in Table II the value for the activation energy lies in the range of the values known from tracer and more indirect resistivity measurements. Q_{MA} is considerably larger than the activation energy for self-diffusion Q_{SD} in Al. This fact is in accordance with the general tendency of the transition impurities Cr, Mn, Fe, and Co in Al,³⁸ the value of the prefactor lies between the values known from the tracer experiments according to the general trend that higher activation energies are accompanied by higher prefactors.

Contrary to all other experiments an earlier Mössbauer study of ⁵⁷Fe diffusion in polycrystalline Al samples¹⁵ yielded an activation energy $Q_{MA} = 1.4$ eV. This value is not very different from Q_{SD} for Al. In this experiment the concentration of the ⁵⁷Fe atoms was very small, about 0.1 at ppm. A preferential trapping of the ⁵⁷Fe atoms in the neighborhood of the grain boundaries seems to be possible. Therefore, we suppose that in the measurements at polycrystalline samples a considerable contribution of enhanced diffusion along the grain boundaries might have influenced the result.

As mentioned in the Introduction anisotropic broadening of the Mössbauer resonance has also been measured for ⁵⁷Fe diffusion in a Cu single crystal.¹⁸ The results are in agreement with the present ones: the angular dependence of Δ_{LW} confirms a NN vacancy diffusion mechanism of the Fe impurity in the Cu matrix, whereas the smoothening of the experimental curve (as large as in the Al ⁵⁷Fe experiment) does not fit with the calculations on the basis of a self-diffusion model. The authors suggested that this smoothening might be caused by divacancy contribution to the diffusion and by correlation effects. They did not perform measurements at temperatures other than 1303 K, i.e., information about a possible change in the anisotropy and a possible Fe-vacancy binding is not available. Without this additional information it appears impossible to fit their data to Eq. (27) in order to check their suggestions, because too many parameters are undetermined.

V. CONCLUSIONS

This study has demonstrated the capability of Mössbauer investigations to yield microscopic information about the geometry and jump frequencies involved in impurity diffusion. In particular the following features are remarkable:

(i) The pronounced anisotropy of the broadening of the Mössbauer resonance for the single-crystal measurements can be explained by diffusion of Fe via exchange jump with nearest-neighbor vacancies.

(ii) The deviation of the measured anisotropy from the curve predicted for the self-diffusion model is evidence for a perturbation of the vacancy jumps in the vicinity of the Fe atom. We have determined the jump frequencies for the five-frequency model (Table III). All vacancy jump frequencies close to an Fe atom turn out to be appreciably smaller than the vacancy jump frequency in pure Al.

(iii) The anomalous decrease of the Mössbauer intensity in the temperature region of diffusion is interpreted with the two-line spectrum predicted by the Krivoglaz model. Only one line, the so-called no-vacancy line, can be detected since the width of the other line is much larger than the frequency range investigated, and its intensity is thus lost in the background. The quantitative analysis yields a binding energy of $E_b \leq 0.29$ eV for the Fe-vacancy complex.

(iv) From the temperature dependence of the line broadening we obtain an activation energy for Fe diffusion in Al $Q_{MA} = 2.3 \pm 0.2$ eV in good agreement with previous results. The absolute value of the broadening is consistent with the value of the

Fe-diffusion coefficient in Al which close to the melting point is much smaller than the self-diffusion coefficient of Al [$D_{MA}/D_{Al}(923\text{ K})=0.24$].

ACKNOWLEDGMENTS

The aluminum single crystal was kindly supplied by M. Abdel Fattah, Institut Für Festkörperfor-

schung Jülich. We thank W. Schilling for generous support of this work and P. H. Dederichs for helpful discussions. We acknowledge the financial support by Deutsche Forschungsgemeinschaft, Sonderforschungsbereich 161 (Hyperfeinwechselwirkungen).

- ¹R. W. Siegel, in *Point Defects and Defect Interactions in Metals*, edited by J. Takamura, M. Doyama, and M. Kiritani (University of Tokyo Press, Tokyo, 1982), p. 533 and references therein.
- ²N. L. Peterson, *J. Nucl. Mater.* **69 & 70**, 3 (1978).
- ³A. D. Le Claire, *J. Nucl. Mater.* **69 & 70**, 70 (1978).
- ⁴K. Hirano, in *Point Defects and Defect Interactions in Metals*, edited by J. Takamura, M. Doyama, and M. Kiritani (University of Tokyo Press, Tokyo, 1982), p. 541 and references therein.
- ⁵K. S. Singwi and A. Sjölander, *Phys. Rev.* **120**, 1093 (1960).
- ⁶M. A. Krivoglaz, *Zh. Eksp. Teor. Fiz.* **40**, 1812 (1961) [*Sov. Phys.—JETP* **13**, 1273 (1961)].
- ⁷C. T. Chudley and R. J. Elliot, *Proc. Phys. Soc., London* **77**, 353 (1961).
- ⁸M. A. Krivoglaz and S. P. Repetskiy, *Fiz. Met. Metalloved.* **32**, 899 (1971) [*Phys. Met. Metallogr. (USSR)* **32**, 1 (1971)].
- ⁹M. C. Dibar-Ure and P. A. Flinn, *Appl. Phys. Lett.* **23**, 587 (1973); *Phys. Rev. B* **15**, 1261 (1977).
- ¹⁰D. Wolf, *Appl. Phys. Lett.* **30**, 617 (1977).
- ¹¹O. Bender and K. Schroeder, *Phys. Rev. B* **12**, 3399 (1979).
- ¹²R. C. Knauer and J. G. Mullen, *Phys. Rev.* **174**, 711 (1968); *Appl. Phys. Lett.* **13**, 150 (1968).
- ¹³S. J. Lewis and P. A. Flinn, *Appl. Phys. Lett.* **15**, 331 (1969).
- ¹⁴S. J. Lewis and P. A. Flinn, *Philos. Mag.* **26**, 977 (1972).
- ¹⁵K. Sørensen and G. Trumphy, *Phys. Rev. B* **7**, 1791 (1973).
- ¹⁶R. Lindsey, *Phys. Status Solidi B* **75**, 583 (1976).
- ¹⁷C. Janot and P. Delcroix, *J. Phys. (Paris)* **62**, 650 (1979).
- ¹⁸S. Asenov, T. Ruskov, T. Tomov, and I. Spirov, *Phys. Lett.* **79A**, 349 (1980).
- ¹⁹S. Mantl, W. Petry, and G. Vogl, in *Nuclear Physics Methods in Materials Research*, edited by K. Bethge et al. (Vieweg, Braunschweig, 1980), p. 427.
- ²⁰M. Blume and J. A. Tjon, *Phys. Rev.* **165**, 446 (1968); *J. A. Tjon and M. Blume, ibid.* **165**, 456 (1968).
- ²¹S. Dattagupta, *Phys. Rev. B* **12**, 3584 (1975).
- ²²As mentioned in the Introduction, the approaching vacancy also causes a quadrupole splitting of the nuclear transition. As known from quenching studies (Ref. 23) this splitting is small in comparison to Γ_0 in the case of vacancies associated to Fe in Al. That is why we can omit the quadrupole interaction in our considerations.
- ²³K. Sassa, H. Gato, Y. Ishida, and M. Kato, *Scr. Metall.* **11**, 1029 (1977).
- ²⁴K. Schroeder (unpublished).
- ²⁵M. Eisenstadt and A. G. Redfield, *Phys. Rev.* **132**, 635 (1963).
- ²⁶D. Wolf, *Phys. Rev. B* **10**, 2710 (1974); **10**, 2734 (1974).
- ²⁷K. Schroeder and D. Wolf (unpublished).
- ²⁸K. Schroeder, D. Wolf, and P. H. Dederichs, in *Point Defects and Defect Interactions in Metals*, edited by J. Takamura, M. Doyama, and M. Kiritani (University of Tokyo Press, Tokyo, 1982), p. 570.
- ²⁹Following Le Claire we assume that in Eq. (7) $e^{S_b/k_B}=1$ with S_b the binding entropy. Furthermore, we have made the usual approximation $E_b \simeq H_b$, where H_b is the binding enthalpy.
- ³⁰D. Wolf and K. Differt, *Comput. Phys. Commun.* **13**, 167 (1977).
- ³¹J. R. Manning, *Diffusion Kinetics for Atoms in Crystals* (Van Nostrand, Princeton, 1968), p. 117.
- ³²T. Springer, *Quasielastic Neutron Scattering for the Investigation of Diffusive Motions in Solids and Liquids, Springer Tracts in Modern Physics, Vol. 64* (Springer, New York, 1972).
- ³³G. M. Hood, *Philos. Mag.* **21**, 305 (1970).
- ³⁴W. B. Alexander and L. M. Slifkin, *Phys. Rev. B* **1**, 3274 (1970).
- ³⁵A. Seeger, D. Wolf, and H. Mehrer, *Phys. Status Solidi B* **48**, 481 (1971).
- ³⁶For solubility the mother ^{57}Co is involved; the diffusion, however, is studied on the daughter ^{57}Fe . When we speak about the diffusion we therefore speak of ^{57}Fe .
- ³⁷M. Hansen and K. L. Anderko, *Constitution of Binary Alloys* (McGraw-Hill, New York, 1958).
- ³⁸G. Erdélyi, D. L. Beke, F. J. Kedves, and I. Gödeny, *Philos. Mag.* **B38**, 445 (1978).
- ³⁹N. Peterson and S. J. Rothman, *Phys. Rev. B* **1**, 3264 (1970).
- ⁴⁰R. S. Preston and R. Gerlach, *Phys. Rev. B* **3**, 1519 (1971).
- ⁴¹W. Petry, G. Vogl, and W. Mansel, *Z. Phys. B* **46**, 319 (1982).
- ⁴²H. Wegener, *Der Mössbauereffekt und seine Anwendung in Physik und Chemie* (Bibliographisches Institut, Mannheim, 1965).
- ⁴³K. Sassa, W. Petry, and G. Vogl, *Philos. Mag. A* (in press).

- ⁴⁴B. von Guérard, H. Peisl, and R. Zitzmann, *Appl. Phys.* **3**, 37 (1974).
- ⁴⁵R. O. Simmons and R. W. Balluffi, *Phys. Rev.* **117**, 62 (1960).
- ⁴⁶Ch. Janot, *J. Phys. (Paris)* **37**, 253 (1976).
- ⁴⁷Measuring the temperature dependence of the entire anisotropy demands forbiddingly long measuring time (> 1 yr). The two orientations $\langle 112 \rangle$ and $\langle 110 \rangle$ are supposed to be representative for other directions in the Brillouin zone.
- ⁴⁸D. Wolf, *Solid State Commun.* **23**, 853 (1977).
- ⁴⁹H. Mehrer, *J. Phys. F* **2**, L11 (1972).
- ⁵⁰N. L. Peterson and S. J. Rothman, *Phys. Rev. B* **17**, 4666 (1978).
- ⁵¹H. S. Berger, S. T. Ockers, M. K. Chason, and R. W. Siegel, *J. Nucl. Mater.* **69 & 70**, 734 (1978).
- ⁵²J. Mundy, private communication.
- ⁵³J. G. Mullen and R. C. Knauer, *Mössbauer Effect Methodology* (Plenum, New York, 1969), Vol. 5, p. 197.
- ⁵⁴H. R. Anand and J. G. Mullen, *Phys. Rev. B* **8**, 3112 (1973).
- ⁵⁵A strong decrease of the Mössbauer line intensity was also found in experiments on ⁵⁷Fe self-diffusion in V-stabilized bcc Fe (Ref. 16). In this case the anomalous decrease cannot be due to an increasing fraction of vacancy-bound ⁵⁷Fe atoms, since the fraction of ⁵⁷Fe atoms coupled to vacancies is small because $c_{\text{NN}}=c_v \simeq 10^{-3}$ at the melting point and thus the contribution of the vacancy line is negligible.
- ⁵⁶P. H. Dederichs and H. Schober, in *Landolt-Börnstein, Zahlenwerte und Funktionen aus Naturwissenschaft und Technik* (Springer, Berlin, 1981), Neue Serie, Vol. 13A, p. 16.
- ⁵⁷A. J. Perry and K. M. Entwistle, *J. Inst. Met.* **96**, 344 (1968).
- ⁵⁸T. S. Lundy and J. F. Murdock, *J. Appl. Phys.* **33**, 1671 (1962).
- ⁵⁹F. Y. Fradin and T. J. Rowland, *Appl. Phys. Lett.* **11**, 207 (1967).
- ⁶⁰H. el Sayed and I. Kovács, *Phys. Status Solidi A* **24**, K45 (1974).
- ⁶¹A. Tonejc, *Philos. Mag.* **27**, 753 (1973).